Impact of horizontal resolution and model time step on European precipitation extremes in the OpenIFS 43r3 atmosphere model

Yingxue Liu[1,2], Joakim Kjellsson[1,2], Abhishek Savita[1] and Wonsun Park[3,4]

[1]GEOMAR Helmholtz Centre for Ocean Research Kiel, Kiel, Germany

[2]Faculty of Mathematics and Natural Sciences, Christian Albrechts University of Kiel, Kiel, Germany

[3]Center for Climate Physics, Institute for Basic Science (IBS), Busan, Republic of Korea

[4]Department of Integrated Climate System Science, Pusan National University, Busan, Republic of Korea

Correspondence to: Yingxue Liu (yiliu@geomar.de)

Abstract: Events of extreme precipitation pose a hazard to many parts of Europe but are typically not well represented in climate models. Here, we evaluate daily extreme precipitation over Europe during 1982–2019 in observations (GPCC), reanalysis (ERA5) and a set of atmosphere-only simulations at low- (100 km), medium- (50 km) and high- (25 km) horizontal resolution and also at different time steps (i.e., 60, 30 and 15 min) using low resolution (100 km) with identical vertical resolutions using OpenIFS (version 43r3). We find that both OpenIFS simulations and reanalysis underestimate the rates of extreme precipitation compared to observations. The biases are largest for the lowest resolution (100 km) and decrease with higher horizontal resolution (50 and 25 km) simulations in all seasons. The sensitivity to horizontal resolution is particularly high in mountain regions (such as the Alps, Scandinavia, Iberian Peninsula), likely linked to the sensitivity of vertical velocity to the representation of topography. The sensitivity of precipitation to model resolution increases dramatically with increasing percentiles, with modest biases in the 70th–80th percentile range and large biases above the 99th percentile range. We also find that precipitation above the 99th percentile mostly consists of large-scale precipitation (~80 %) in winter, while in summer it is mostly large-scale precipitation in Northern Europe (~70 %) and convective precipitation in Southern Europe (~70 %). Convective precipitation is more sensitive to model time step than to horizontal resolution. Large-scale precipitation increases significantly with both higher horizontal resolution and shorter model time step.

1. Introduction

Extreme precipitation events have severe impacts on our society and ecosystems. For example, extreme precipitation caused a devastating flood in Germany in 2021, in which around 180 people died. The frequency and intensity of extreme precipitation are projected to increase over most regions in the future (Intergovernmental Panel on Climate Change, 2023; Li et al., 2021; Myhre et al., 2019). The increasing extreme precipitation poses a threat to society and must thus be realistically simulated and projected accurately for future climates. However, the climate models have large biases in simulating extreme precipitation events due to coarse horizontal resolution grid and long model time step etc. (Alexander et al., 2019; Avila et al., 2015; Sillmann et al., 2013). The model biases are also hard to evaluate as we lack long-term observations. This study aims to understand the sensitivity of extreme precipitation to model horizontal resolution and model time step.

Extreme precipitation events are usually underestimated in CMIP models (O'Gorman, 2015; Sillmann et al., 2013). Some studies found the simulated extreme precipitation at higher atmosphere horizontal resolutions is more realistic (Wehner et al., 2010, 2014). Jong et al. (2023) found that the characteristics of extreme precipitation at 25 km resolution configurations have smaller biases that at 50 and 100 km. While, Kopparla et al. (2013) found that the reduced extreme precipitation biases at higher horizontal resolution do not hold for all regions (e.g., Australia).

Strandberg and Lind (2021) reported the effect of horizontal resolution on European extreme precipitation is largest in regions with complex topography and in the summer season when precipitation is mostly caused by convective processes using coupled models, in agreement with Iles et al. (2020). However, Li et al. (2011) demonstrated that the impact of horizontal resolution on global precipitation extremes is manifested mostly by its effects on large-scale precipitation, which could be due to the improved large-scale circulation (Hack et al., 2006). Other studies also found an increasing large-scale precipitation with higher resolution but the convective precipitation is rather insensitive to resolution (Bacmeister et al., 2014; Jung et al., 2012; Kopparla et al., 2013).

67 Both the individual physical parameterization in models and their coupling to the dynamics
68 can benefit from a shorter time step (Jung et al., 2012). Mishra and Sahany (2011) found a
69 more realistic simulation of the heavy precipitation in the tropics when the time step was
70 shortened from 60 to 5 minutes at a coarse (~300 km) resolution in a short-period (12 months)
71 configuration. Jung et al. (2012) also reported that the biases in tropical circulation are smaller
72 at 15 minutes than 60 minutes in the IFS model, which is related to tropical precipitation
73 although they did not work on the precipitation in their study. However, Roberts et al. (2018)
74 found a minimal impact on model biases when shortening the time step from 20 to 15 minutes
75 at 25 km in the IFS model. They either did not investigate the multi-year precipitation extremes,
76 or did not explore the extremes in IFS model.

77 The sensitivity of climate model performance to horizontal resolution and model time step
78 exists in many models, but the level of sensitivity varies considerably between models and
79 studied regions. Most of the global atmosphere-models do not explicitly resolve all the physical
80 processes and must therefore employ parametrizations to represent those unresolved processes
81 (spatially or temporally), which shows a weakness in the models. A recent study by Savita et
82 al. (2024) explored the sensitivity of global mean precipitation to the horizontal resolution and
83 model time step in atmosphere-only simulations with OpenIFS. However, the extreme
84 precipitation's sensitivity to horizontal resolution and time step was not investigated. In this
85 study, we investigated the impact of horizontal resolutions (~100 km, ~50 km, and ~25 km)
86 and model time steps (60 minutes, 30 minutes, and 15 minutes) on daily extreme precipitation
87 using OpenIFS simulations and compare them with observation. We also studied the
88 convective and large-scale precipitation in all simulations. Precipitation extremes sensitivity to
89 model time step is the first time explored in this work using 100 km in OpenIFS atmosphere
90 model. Besides the extremes, we also explored multi-percentile precipitation's sensitivity to
91 horizontal resolution and time step. This paper is structured as follows: section 2 describes the
92 data and methodology, and section 3 discusses the results. The conclusion and discussion can
93 be found in section 4.

94
95
96
97
98
99

2. Data and Methods

2.1 Model, observation, and reanalysis data

The OpenIFS is derived from the Integrated Forecasting System at the European Centre for Medium-range Weather Forecasting (ECMWF-IFS) cycle 43 release 3 (43r3) (ECMWF, 2017). We use the same AMIP simulations that were used in Savita et al. (2024) which cover the period 1979-2014 and are extended to 2019 using sea-surface temperature (SST) from ERA5 and the Shared Socioeconomic Pathway 5 (SSP5-8.5) scenario from CMIP6. OpenIFS simulations use 91 vertical levels (L91) and the different horizontal resolutions: low resolution (Tco95, ~100 km), medium resolution (Tco199, ~50 km), and high resolution (Tco399, ~25 km). For the low resolution, additional sensitivity experiments use different model time steps i.e., 60, 30, and 15 minutes and we refer to these experiments as LR60m, LR30m, and LR, respectively. For medium and high resolution, the same model time step is used (i.e., 15 minutes), of which experiments refer to as MR and HR, respectively. While the OpenIFS uses a reduced octahedral grid (Malardel et al., 2016), the final output used in this study has been interpolated to a regular grid using the second-order conservative method (Kritsikis et al., 2017) by XIOS output server. The LR, LR30m and LR60m output were interpolated to a global 0.9° regular grid while the MR and HR output were interpolated to a global 0.45° regular grid, i.e., we are not investigating extreme precipitation in high resolution simulations in their native reduced octahedral grid, which will be investigated in future study. The simulations used here were used by Savita et al. (2024) who found improvements in the surface zonal wind, Rossby wave amplitude and phase speed, weather regime patterns, and surface-air temperature when shortening a model time step from 60 minutes to 30 and 15 minutes in low resolution or increasing the horizontal resolution from 100 km to 50 and 25 km. However, Savita et al. (2024) did not find such improvement in the mean precipitation bias by increasing horizontal resolution or shortening the model time step.

To validate OpenIFS simulations, we use the gridded daily precipitation observational data from Global Precipitation Climatology Centre (GPCC) with resolution of $1° \times 1°$ for the period 1982−2019 (Ziese et al., 2022) as well as the reanalysis data from the ECMWF Reanalysis v5 (ERA5) for 1979−2019 (Hersbach et al., 2023). ERA5 is based on the IFS Cy41r2, with 31 km horizontal resolution and 137 levels (Hersbach et al., 2020). We analyzed total, large-scale, and convective precipitation in this study. The total precipitation (convective plus large-scale

precipitation) in the IFS is the accumulated precipitation, comprising of rain and snow, that falls to the Earth's surface, and it is not assimilated in the IFS. The convective precipitation is generated by the convection scheme in the IFS, which represents convection at spatial scales smaller than the grid box. The convection scheme follows Sundqvist (1978), which is also used in the OpenIFS. The large-scale precipitation is generated by the cloud scheme (Khairoutdinov and Kogan, 2000), which represents the formation and dissipation of clouds and large-scale precipitation due to changes in atmospheric quantities (such as pressure, temperature, and moisture) predicted directly by the IFS at spatial scales of the grid box or larger. The autoconversion/accretion parameterization is a non-linear function of the mass of both liquid cloud and rainwater. The calculation follows Khairoutdinov and Kogan (2000) which is derived from large eddy simulation studies of drizzling stratocumulus clouds, and this scheme is also used in OpenIFS. Several studies have evaluated the performance of ERA5 and found that the total precipitation in ERA5 is performing well over the US (Tarek et al., 2020; Xu et al., 2019). For global precipitation, the mean absolute difference over 50° S–50° N between ERA5 and TRMM/3B43 is 0.58 mm/d; the global-mean correlation with GPCP data is 0.77, which is better compared to ERA-Interim (0.63 mm/d and 0.67) (Hersbach et al., 2020). ERA5 also performs well in polar regions in representing wind, temperature and humidity (Graham et al., 2019; Tetzner et al., 2019; Wang et al., 2019).

Here we analyze daily ERA5 and the OpenIFS data over Europe (30° N–72° N, 10° W–40° E) for the period of 1982–2019 to be consistent with the GPCC dataset. For comparison, the ERA5, GPCC, MR, and HR data are remapped to LR (~0.9375° × 0.9375°) using the second-order conservative remapping method, which is consistent with the XIOS server used. The second-order conservative method includes the gradient across the source cell, which is not included in the first-order conservative method. Therefore, it gives a smoother, more accurate representation of the source field (Jones, 1998).

2.2 Methods

Calculation of qth percentile value

We calculated different percentile values using total precipitation from GPCC, ERA5, and OpenIFS simulations. When we calculated the qth percentile value, the normalized ranking usually did not match the location of the qth percentile exactly, which means the qth lies between two indices. Therefore, we determined the location first, then computed the qth value by

165   interpolating between the two nearest values based on the location. Here we used the formula

166   below to find the location:

167    $$j = q*(n-1) \tag{1}$$

168   *n* is the length of the sample, *q* is the desired percentile, *j* is the location which is the distance

169   from the first value X_1 (X_m are the sorted sample values, *m*=1, 2, …, *n*). Then we took *i* as the

170   nearest (lower) integer of *j* to get the *q*th value P(q) by interpolating.

171    $$P(q) = X_i + (X_{i+1} - X_i) * (j-i) \tag{2}$$

172   There are other methods to determine the location of *q*th percentile (Hyndman and Fan, 1996),

173   but here we use the 'linear' one.

174

175   **The large-scale precipitation contribution to extreme precipitation**

176   To calculate the contribution of large-scale precipitation to total precipitation for a percentile

177   range, at each grid point we accumulated the large-scale precipitation on all days when the total

178   precipitation is in that percentile range, then divided it by the accumulated total precipitation

179   on those days to get the fraction of large-scale precipitation.

180

181   **Calculation of RMSE values**

182   We used the root-mean-square error (RMSE) referenced to GPCC that measures the

183   performance of ERA5 and OpenIFS simulations:

184    $$\mathrm{RMSE} = \sqrt{\frac{\sum_{i=1}^{n}(x_{mi}-x_{oi})^2}{n}} \tag{3}$$

185   x_{mi} is the value at *i* grid point for ERA5 or OpenIFS simulations, x_{oi} is the value for GPCC, *n*

186   is the number of land grid points over Europe. Using equation (3), we calculated the RMSE

187   values for different percentile ranges. Smaller RMSE values mean the biases between OpenIFS

188   (or ERA5) and GPCC are smaller i.e., the model simulations and ERA5 are performing better.

189   The relative RMSE (RRMSE) is calculated by dividing the RMSE by GPCC precipitation at

190   corresponding percentile range.

191

192   **Confidence intervals**

193   We calculated the 2.5 to 97.5th confidence intervals (CI) for the RMSE for each percentile with

194   a bootstrap method. For example, to calculate the CI for the RMSE of HR (referenced to GPCC

195   observation), we randomly chose *n* grid cell pairs from GPCC and HR over European land,

196   then calculated their RMSE (*n* is the number of total land grid points over Europe). This process

197   was repeated for *2000* times. We took the 2.5th and 97.5th percentiles of the distribution of the

198 2000 RMSEs as the 95 % CI. If the CI for different simulations do not overlap then we refer

199 that they are significantly different.

200

3. Results

201

202

3.1 Extreme precipitation over Europe

203

204

205 We show the time series of 99th percentile precipitation calculated from all grid points and all

206 days in each year over the period 1982–2019 from GPCC, ERA5, and OpenIFS simulations

207 over Europe (Fig. 1). The ERA5 simulates an inter-annual variability of the 99th percentile

208 precipitation similar to that in GPCC. For example, the peak in 2010 and the low in 1994 are

209 well reproduced in the ERA5. ERA5 is a reanalysis product that assimilates observation of

210 precipitation, therefore, we expect it to do a better job of reproducing dry (1994) and wet (2010)

211 years than OpenIFS simulations that do not reproduce the same inter-annual variability as in

212 GPCC or ERA5. However, LR and HR do reproduce the 95 % significant positive trend

213 observed in GPCC (0.03 mm/d/y, not shown), which are ~0.02 mm/d/y for both LR and HR,

214 and it is not significant for MR. We note that the OpenIFS simulations use observed SST and

215 sea-ice concentrations as boundary conditions, but ozone is taken from a photochemical

216 equilibrium (Cariolle and Teyssèdre, 2007) and aerosol concentrations are taken from

217 Copernicus Atmosphere Monitoring Service (CAMS) monthly climatology. Therefore, we do

218 not expect LR, MR and HR to reproduce trends driven by ozone or aerosols forcing. We also

219 find that both ERA5 and OpenIFS simulations have relatively lower 99th percentile

220 precipitation rates compared to GPCC (Fig. 1). The RMSE for ERA5 (0.36 mm/d) is lower

221 than for OpenIFS simulations which is largest for LR (2.03 mm/d) and decreases with higher

222 horizontal resolution (i.e., 1.13 mm/d for MR and 0.69 mm/d for HR). Note that Fig. 1 does

223 not contain any spatial information and that a mismatch between model data and observations

224 can be due to the 99th percentile occurring in different regions and/or with different magnitudes.

225 The RMSE analysis suggests that ERA5 and HR are close to GPCC and LR is far from GPCC.

226

227 Figure 2a–e shows the spatial distribution of the 99th percentile precipitation over Europe for

228 all days in each season for all years in GPCC, ERA5, and OpenIFS simulations, respectively.

229 In general, the extreme precipitation is very low (~ 2 mm/d) in Northern Africa, which is to be

230 expected since the mean precipitation is only 0.5 mm/d in those regions (Fig. S1). The extreme

231 precipitation exceeds 30 mm/d over mountain areas (e.g., Scandinavian mountains, Alps, and

232 Iberian Peninsula) and the north coast of the Mediterranean but is otherwise lower (~15 mm/d).

The spatial distribution of extreme precipitation matches that of the mean precipitation pattern (Fig. S1). The high 99th percentile precipitation near mountains is likely due to the forced ascent of westerly (Scandinavia, Iberian Peninsula, British Isles) and southerly (Alps) winds. The high 99th percentile precipitation in the north of the Mediterranean is likely because of warm and moist southerly winds from the Mediterranean Sea. The ERA5 and OpenIFS simulations overall reproduce the spatial distribution of the 99th percentile precipitation from GPCC. However, the magnitudes are different, particularly over the Scandinavian mountains, the Alps, and central Europe near 50° N (Fig. 2a–e). Figure 2f–i show the regional biases for the 99th percentile precipitation referenced to GPCC. LR mostly underestimates the 99th percentile precipitation in mountainous areas and deserts by more than 25 % (Fig. 2g) and the biases are reduced when horizontal resolution is increased in MR and HR (Fig. 2h–i). We also notice that LR underestimates the 99th percentile precipitation south of the Alps but overestimates it to the north (Fig. 2 (g)), whereas this bias is negligible in higher-resolution simulations (Fig. 2h–i). This is due to the lower and gentler Alps region simulated in LR (Fig. S2), where the moist southerly winds do not ascend high enough, therefore there is less precipitation formed on the southern side and more moisture is advected over the mountain. The moist air descends more slowly over gentler leeward side in LR than MR (HR), thus the leeward region may get more precipitation. The reduced biases near mountain regions in the higher-resolution simulations are likely because higher resolution has a better representation of topography and vertical velocity. A cross section of the topography and annual-mean vertical velocity at 850 hPa and 62° N (Fig. S3a&b) highlight that the higher-resolution simulations resolve steeper topography, which leads to more ascent and thus more precipitation.

The 99th percentile precipitation over the Alps is more realistic with higher horizontal resolution compared to lower resolution. However, all simulations as well as ERA5 exhibit a negative bias over northeast Italy and west Slovenia (Fig. 2f–i). By analyzing the EOBS data, we find a similar negative bias as in GPCC, but a positive bias in GPCP (Fig. S4d-k). We notice that the extreme precipitation over the Alps (including Slovenia) in GPCP is lower than GPCC and EOBS (Fig. S4a-c), which is likely due to the different data sources and grid methods in different observation datasets (e.g., GPCC and EOBS are gauge-based gridded data on the land, but GPCP data combines microwave and infrared measurements, satellites and rain gauges). We do not know which observation dataset is more realistic, therefore, the cause of the negative bias near Slovenia could be a bias in GPCC or a persistent model bias in the ECMWF-IFS on

266   which both ERA5 and OpenIFS are based. In general, ERA5 has a lower RMSE (2.6 mm/d)

267   for extreme total precipitation than OpenIFS simulations, i.e., ERA5 has overall lower biases

268   than LR (4.0 mm/d) and is similar to MR (3.0 mm/d) and HR (2.9 mm/d).

269

270   We next calculate the trend for the annual 99th percentile precipitation over Europe (Fig. 3 &

271   4) and find that the 99th percentile precipitation has a large positive trend in central Europe and

272   a negative trend to the north of the Alps in GPCC (Fig. 3a). The ERA5 reproduces the pattern

273   of the trend found in GPCC but is not significant. However, OpenIFS simulations do not have

274   consistent patterns with GPCC (Fig. 3d–f, Fig. 4d–f), with only LR30m reproducing the large

275   positive trend in central Europe (Fig. 4d). Overall, the trend is largely underestimated over

276   central Europe but overestimated over northern Europe in OpenIFS simulations. We have not

277   found any consistent improvement across the horizontal resolution and model time step.

278

279   In addition to the 99th percentile precipitation and the trend, we calculate annual total

280   precipitation in different percentile ranges, such as 70th–80th, 80th–90th, 90th–95th, 95th–99th,

281   99th–99.5th, 99.5th–99.9th and larger than 99.9th (i.e., >99.9th) percentile. The RMSEs for ERA5

282   and OpenIFS simulations referenced to GPCC in each range are shown in Fig. 5. The RMSEs

283   increase exponentially with increasing percentiles, from less than 1 mm/d at the 70th–80th

284   percentile range to ~8 mm/d above the 99.9th percentile range. The largest RMSE is found for

285   LR60m above the 99.9th percentile range which is around 12 mm/d [CI: 11.3–12.8 mm/d]. We

286   also find that the RMSEs decrease with finer horizontal resolution for all percentile ranges. The

287   CI of the RMSEs from LR do not overlap with those from higher horizontal resolutions for any

288   percentile range, i.e., the biases from LR are significantly different from that at higher

289   resolutions and thus clearly sensitive to the horizontal resolution. Notably, the RMSE

290   differences between LR simulation and the higher-resolution simulations as well as ERA5 are

291   larger at higher percentile ranges (>95th) than those at lower percentile ranges (<95th). This

292   suggests that the extreme precipitation is more sensitive to horizontal resolution than

293   precipitation at lower percentile ranges (<95th). ERA5 has the smallest RMSE of all datasets

294   above the 95th percentile ranges, i.e., ERA5 has a better representation of the extreme

295   precipitation than our OpenIFS simulations (Fig. 5).

296

297   The RMSEs for LR60m, LR30m, and LR are smaller when the model time step is shorter.

298   However, the CI of RMSE overlaps at all percentile ranges, i.e., the sensitivity of precipitation

to the model time step is not statistically significant in the low-resolution configurations. While the model time step may influence precipitation, especially convective precipitation, errors from poorly resolved topography probably have a large impact on the RMSE, which would explain the lack of sensitivity to the model time step.

The above analysis is based on the RMSE values, which measure the absolute magnitude of biases. The exponential increase in RMSE with higher percentiles is due to the corresponding exponential increase in precipitation amounts across those percentiles. The relative biases are further explored by calculating the relative RMSE (RRMSE) (Fig. S5). For the precipitation above 90th percentile (> 6 mm/d), RRMSEs are larger at higher percentiles (>99.9th percentile) than lower percentiles (90-95th percentile). A larger sensitivity to horizontal resolution at higher percentiles can be also seen, since the RRMSE differences between LR and MR (HR) slightly increase from 5.5% at 90-95th to 6.9% above 99.9th percentile. The above RRMSEs' results are qualitatively consistent with the larger RMSE and sensitivity to horizontal resolution at higher percentiles shown in Fig. 5, but quantitatively RRMSE shows smaller variations across percentiles than RMSE does. However, the RRMSE at 70-90th percentile ranges show comparable magnitude and sensitivity to those above 99th percentile, which is related to the very low precipitation amounts at these percentiles (1.9 mm/d for 70-80th and 3.6 mm/d for 80-90th percentile range).

3.2 Relative roles of convective and large-scale precipitation

Total precipitation is the sum of convective and large-scale precipitation. Convective precipitation is related to unresolved convective motions. It comes from the physical processes whose scales are smaller than the resolution of the model, therefore need to be parametrized. On the other hand, large-scale precipitation is related to large-scale processes larger than the model resolution, that can be resolved. When moving to higher horizontal resolutions, large-scale precipitation is likely to increase, and the ratio between convective and large-scale precipitation may change. In this section we split the extreme precipitation into convective and large-scale precipitation to see their sensitivities to horizontal resolution and model time step. The extreme precipitation is nearly 100 % large-scale precipitation over northern Europe, more than 90 % over central Europe, and more than 70 % over western and southern Europe in DJF (Fig. 6e–h). However, in JJA the extreme precipitation is mostly large-scale precipitation over northern Europe (>70 %) and convective precipitation in the Mediterranean region (>70 %)

333   (Fig. 6a–d). Due to the seasonal dependent large-scale precipitation contribution to extreme

334   total precipitation, we discuss convective and large-scale precipitation's sensitivities to

335   horizontal resolution and time step in JJA and DJF separately. The ratios between convective

336   and large-scale precipitation are also discussed here. Considering the ratios over parts of

337   Mediterranean region are very large, which influence the results a lot, we remove that region

338   and only include the region north than 40°N (i.e., 40° N–72° N, 10° W–40° E) in this section.

339

340   During the extreme precipitation days, Europe has more convective precipitation in JJA (~10

341   mm/d) than in DJF (~3.7 mm/d), and their distributions do not change much across horizontal

342   resolution (Fig. 7a & b). While, from the significant test (Table 2a), we found JJA convective

343   precipitation only increases significantly moving from MR to HR, and DJF convective

344   precipitation significantly increases from LR to MR (HR). However, convective precipitation's

345   distributions vary noticeably across model time steps, as shown in Fig. 7 c & d. As the model

346   time step reduces, the distributions of JJA convective precipitation move to the left, thus less

347   convective precipitation are simulated in shorter time step simulations. DJF has similar results

348   as in JJA. The changes are significant (Table 2a), that is, convective precipitation in OpenIFS

349   is sensitive to model time step.

350

351   The distributions of large-scale precipitation in MR and HR (Fig. 7e) shift to the right compared

352   to LR in JJA, and MR and HR have significantly more large-scale precipitation (13.2 mm/d)

353   than LR (11.4 mm/d). In DJF, the distribution peak of LR, MR and HR are similar (Fig. 7f),

354   but MR and HR have bigger tails than LR. Thus, MR and HR have more large-scale

355   precipitation than LR. The increase of large-scale precipitation is likely due to the better

356   simulated topography at higher horizontal resolution, where more large-scale precipitation is

357   resolved. The changes of large-scale precipitation in both JJA and DJF from LR to MR are

358   significant, but not from MR to HR (Table 2b). That means, the large-scale precipitation is

359   sensitive when horizontal resolution is increased from LR to MR, but not from MR to HR.

360   Large-scale precipitation also significantly increases when the model time step is shorten from

361   60 min to 30 min, and also from 30 min to 15 min in both JJA (Fig. 7g) and DJF (Fig. 7h), that

362   is large-scale precipitation is also sensitive to the model time step.

363

364   We further analyse the distribution of ratio between convective and large-scale precipitation in

365   JJA and DJF, shown in Fig. 8. For different resolutions, the ratio distributions from MR and

366   HR are narrower and slightly shift to the left compared to LR in JJA (Fig. 8a), which means

367   MR and HR have smaller mean ratios (1.5) than LR (~1.25). That is due to the large-scale

368   precipitation increasing by 16% with finer horizontal resolution, whereas convective

369   precipitation only increases by 6%. However, the ratio between convective and large-scale

370   precipitation do not vary significantly with higher horizontal resolutions in DJF (Fig. 8b).

371   When moving to shorter model time step, the ratios significantly decrease in JJA (from 2 to

372   1.5) and DJF (Fig. 8c-d, Table 2c). It is related to the significant decreasing convective and

373   increasing large-scale precipitation with shorter model time step.

374

375   In summary, during extreme precipitation days, large-scale precipitation increases with higher

376   horizontal resolution and shorter model time step; however, convective precipitation increases

377   with higher horizontal resolution and decrease with shorter model time step. Convective

378   precipitation is more sensitive to model time steps than to horizontal resolutions, while large-

379   scale precipitation is sensitive to both. Therefore, the extreme precipitation sensitivity to

380   horizontal resolution is mostly from large-scale precipitation.

381

382   We also analyse the mean state convective and large-scale precipitation's sensitivity to

383   horizontal resolution and model time step (Fig. S6 & S7). Convective precipitation decreases

384   and large-scale precipitation increases with higher horizontal resolution and shorter model time

385   step, therefore their ratio decreases. Their sensitivities to resolutions and time steps are less

386   significant in mean state than in extreme state, especially for mean convective precipitation,

387   which is only significantly sensitive when shortening model time step from 30 min to 15 min.

388   The changes of mean convective precipitation with horizontal resolution are opposite with the

389   extreme one (Fig. S6a & b, Fig. 7a & b), but these changes for both extreme and mean states

390   are very little, and convective precipitation is more sensitive to model time steps in both states

391   (Fig. S6c & d, Fig. 7c & d).

392

393   **4. Discussion and Conclusion**

394   We have investigated the sensitivity of extreme precipitation across different horizontal

395   resolutions and model time steps in atmosphere-only experiments with the OpenIFS.

396   Comparing extreme precipitation (defined as total daily precipitation at the 99th percentile)

397   from OpenIFS simulations, reanalysis (ERA5), and observation (GPCC), we find that MR and

398   HR mostly better represent the precipitation extremes compared to LR. We also found a more

399   significant sensitivity to the horizontal resolution for the precipitation above the 95th percentile

400   and less sensitivity for lower percentile ranges (<95th) (Fig. 5). These OpenIFS-based results

401 are similar to Kopparla et al. (2013), who found that the bias of extreme precipitation in the

402 high-resolution simulation (25 km) is reduced compared to the lower-resolution simulations

403 (100 km and 200 km) over Europe in their atmospheric model, but not for precipitation at lower

404 percentiles (i.e., <95th). However, the sensitivity to the horizontal resolution found by Kopparla

405 et al. (2013) was not significant over Europe which is rather different from our results as we

406 have found a significant difference across the horizontal resolutions. In contrast to the extreme

407 precipitation, the bias for global mean precipitation is not decreasing much with higher

408 horizontal resolution in OpenIFS. Similar results are also found in other AGCMs (e.g.,

409 ECHAM6, OpenIFS, HadGEM1 and HadGEM3) (Hertwig et al., 2015; Savita et al., 2024;

410 Schiemann et al., 2014; Demory et al., 2020;). However, Delworth et al. (2012) found an

411 improvement in the global mean precipitation with higher horizontal resolution in a coupled

412 model (GFDL).

413

414 The improvements due to higher horizontal resolution for the extreme precipitation are mostly

415 over the mountain areas, consistent with previous studies which found the effect of horizontal

416 resolution being largest in areas with complex topography over Europe and also other regions

417 for mean and extreme precipitation (Demory et al., 2020; Iles et al., 2020; Monerie et al., 2020;

418 Prein et al., 2013; Torma et al., 2015). The sensitivity to the horizontal resolution comes from

419 the large-scale precipitation, which is likely because of the better-resolved topography.

420 However, the convective precipitation is more sensitive to the model time step than it is to the

421 horizontal resolution.

422

423 In our results, larger improvements are obtained when the horizontal resolution is increased

424 from LR to MR, but relatively smaller improvements from MR to HR. This diminishing return

425 is also found by Roberts et al. (2018) from ~50 km to ~25 km in ECMWF-IFS, but for

426 climatological surface biases. The simulation of extratropical cyclones, tropospheric

427 circulation and tropical mean precipitation in ECMWF-IFS also have smaller improvements

428 from 39 km to 16 km than that from 126 km to 39 km (Jung et al., 2012). However, the tropical

429 cyclone intensity and intense storm structure, which often cause extreme precipitation in tropics

430 (Gori et al., 2022; Zhu and Quiring, 2022) are adequately simulated at 16 km, but not at 126

431 and 39 km resolutions in ECMWF-IFS (Manganello et al., 2012). Therefore, the diminishing

432 return in this study is valid for European extreme precipitation, but may not for tropical extreme

433 precipitation.

434

435   Since the analysis of horizontal resolution's impact is based on regridded data, it may therefore

436   be influenced by the regridding process. The native resolution of our model output is 192×384

437   for LR, 400×800 for MR and 800×1600 for HR; however, only 400×800 for HR output is saved

438   due to computational cost.   Similar to the result of regridded data (Fig. 1), extreme

439   precipitation on their native resolution is underestimated in OpenIFS compared to GPCC, and

440   the biases decrease with higher horizontal resolution (Fig. 9). Extreme precipitation on native

441   resolutions also has similar spatial distribution with that on regridded resolution (Fig. 10, Fig.

442   2), such as more extreme precipitation in mountain areas. However, the extreme precipitation

443   is larger (13% for GPCC, 7% for MR and 12% HR) on native resolution than on regridded

444   resolution, because some extreme precipitation is smoothed when regridding to 0.9×0.9

445   degree. The RMSEs of extreme precipitation against GPCC are also larger on native resolution

446   (Fig. 9) than on regridded resolution (Fig. 1), which holds across different percentiles (Fig. S8).

447   Moreover, the sensitivity of extreme precipitation to horizontal resolution is also greater on

448   native resolution (Fig. S8).   Convective and large-scale precipitation during extreme

449   precipitation days increase with higher horizontal resolution (Fig. 11 a-d), consistent with

450   regridded results. The convective-to-large-scale precipitation ratio significantly decreases from

451   LR to MR in JJA (Fig. 11e), which is also consistent with regridded results. However, the ratio

452   increases from MR to HR in JJA on native resolution, differing from regridded analysis, likely

453   due to the dramatic increasing convective precipitation from MR to HR in JJA. Overall,

454   regridding the model dataset does not change the conclusion qualitatively in this study but

455   causes quantitative differences.

456

457   Moreover, the choice of observation dataset is a key factor for assessing the impact of the

458   horizontal resolution and model time step on extreme precipitation. Most observation

459   precipitation data are from one of the three categories, gauge-based products, satellite products,

460   and merged satellite-gauge products. Since the satellite products are constructed with satellite

461   microwave and/ or infrared measurements, with/ without gauged-adjusted estimates,

462   differences exist between these products. Besides, the gauge-based products are highly

463   dependent on the choice of stations and interpolation schemes. It is hard to say which product

464   is closer to reality, as different regions may have different observation datasets that suit best

465   for the analysis. In particular, we note that not all products are suitable for extreme analysis.

466   For example, GPCP's main scope is to construct a reliable climate data record and has been

467   developed with a priority of ensuring the long-term stability of data (Adler et al., 2017).

468   Masunaga et al. (2019) found that the frequency of GPCP daily precipitation quickly drops

469 below all other datasets once the precipitation exceeds 30 mm/d. Also, the time series of GPCP

470 extreme precipitation over the ocean exhibits a jump to lower 99th percentiles in late 2008/early

471 2009 which is not present in all other datasets, coinciding with the change in utilization of

472 SSM/I and SSMIS. The lower 99th precipitation suggests that the GPCP dataset might not be

473 applied to extreme analysis (Masunaga et al., 2019). Therefore, we only use GPCC observation

474 data as the reference to explore the model performance. In Fig. 2f–i the 99th percentile

475 precipitation is largely underestimated in the eastern Alp region by ERA5 and all model

476 simulations. The biases are insensitive to horizontal resolution. It is likely a persistent model

477 bias in the ECMWF-IFS or a bias in GPCC. Comparing model output to multiple observational

478 precipitation products instead of relying on a single one may be a good way to reduce these

479 biases. Multiple observational products can be taken as an ensemble, which provide a spread

480 of observational estimates and allow insights into whether and which model configurations sit

481 within this observational spread.

482

483 **Code and data variability**

484 The OpenIFS model requires a software license agreement with ECMWF to use it, and

485 OpenIFS's license is easily given free of charge to any academic or research institute. The

486 details of OpenIFS are available at

487 https://confluence.ecmwf.int/display/OIFS/About+OpenIFS (ECMWF, 2018). We used the

488 same simulation that used in Savita et al. (2024) and therefore do not provide the data needed

489 to reproduce the simulations here. All data (runscripts, input data etc) needed to reproduce the

490 simulations can be found in Savita et al. (2024) in code and data variability section. The jupyter

491 notebook scripts used in this study to produce the plots can be found at

492 https://doi.org/10.5281/zenodo.15497274. The raw model output is available from the authors

493 upon reasonable request. The observation and reanalysis datasets used in this study can be

494 downloaded from GPCC (https://opendata.dwd.de/climate_environment/GPCC/html/fulldata-

495 daily_v2022_doi_download.html, Ziese et al., 2022) and ERA5

496 (https://cds.climate.copernicus.eu/cdsapp#!/dataset/reanalysis-era5-single-levels?tab=form,

497 Hersbach et al., 2023).

498

499 **Authors contributions.** AS and JK conducted all the OpenIFS simulations. YL did the

500 analysis and writing with substantial contribution from JK, AS and WP.

501

502 **Competing interests.** The contact author has declared that none of the authors has any
503 competing interests.
504
505 **Acknowledgements.** Yingxue Liu is supported by China Scholarship Council (CSC, grant no.
506 202004910401). Joakim Kjellsson and Abhishek Savita are supported by JPI Climate/Ocean
507 (ROADMAP project, grant no. 01LP2002C). Wonsun Park was supported by IBS (grant no.
508 IBS-R028-D1). We thank the OpenIFS team at ECMWF for the technical support. All the
509 OpenIFS simulations were conducted on the HLRN machine under shk00018 project resources.
510 All the analysis and data storage were conducted on computer clusters at GEOMAR and Kiel
511 University Computing Center (NESH).
512
513 **Financial support.** This research is financially supported by CSC (grant no. 202004910401)
514 and ROADMAP project (grant no. 01LP2002C).
515
516
517
518
519
520
521
522
523
524
525
526
527
528
529
530
531
532
533
534

535

References

537 Adler, R. F., Gu, G., Sapiano, M., Wang, J. J., and Huffman, G. J.: Global Precipitation:
538   Means, Variations and Trends During the Satellite Era (1979–2014),
539   https://doi.org/10.1007/s10712-017-9416-4, 1 July 2017.
540 Alexander, L. V., Fowler, H. J., Bador, M., Behrangi, A., Donat, M. G., Dunn, R., Funk,
541   C., Goldie, J., Lewis, E., Rogé, M., Seneviratne, S. I., and Venugopal, V.: On the use of
542   indices to study extreme precipitation on sub-daily and daily timescales, Environmental
543   Research Letters, 14, https://doi.org/10.1088/1748-9326/ab51b6, 2019.
544 Avila, F. B., Dong, S., Menang, K. P., Rajczak, J., Renom, M., Donat, M. G., and
545   Alexander, L. V.: Systematic investigation of gridding-related scaling effects on annual
546   statistics of daily temperature and precipitation maxima: A case study for south-east
547   Australia, Weather Clim Extrem, 9, 6–16, https://doi.org/10.1016/j.wace.2015.06.003,
548   2015.
549 Bacmeister, J. T., Wehner, M. F., Neale, R. B., Gettelman, A., Hannay, C., Lauritzen, P.
550   H., Caron, J. M., and Truesdale, J. E.: Exploratory high-resolution climate simulations
551   using the community atmosphere model (CAM), J Clim, 27, 3073–3099,
552   https://doi.org/10.1175/JCLI-D-13-00387.1, 2014.
553 Bell, B., Hersbach, H., Simmons, A., Berrisford, P., Dahlgren, P., Horányi, A., Muñoz-
554   Sabater, J., Nicolas, J., Radu, R., Schepers, D., Soci, C., Villaume, S., Bidlot, J. R.,
555   Haimberger, L., Woollen, J., Buontempo, C., and Thépaut, J. N.: The ERA5 global
556   reanalysis: Preliminary extension to 1950, Quarterly Journal of the Royal
557   Meteorological Society, 147, 4186–4227, https://doi.org/10.1002/qj.4174, 2021.
558 Cariolle, D. and Teyssèdre, H.: Atmospheric Chemistry and Physics A revised linear ozone
559   photochemistry parameterization for use in transport and general circulation models:
560   multi-annual simulations, Atmos. Chem. Phys, 2183–2196 pp., 2007.
561 Delworth, T. L., Rosati, A., Anderson, W., Adcroft, A. J., Balaji, V., Benson, R., Dixon,
562   K., Griffies, S. M., Lee, H. C., Pacanowski, R. C., Vecchi, G. A., Wittenberg, A. T.,
563   Zeng, F., and Zhang, R.: Simulated climate and climate change in the GFDL CM2.5
564   high-resolution coupled climate model, J Clim, 25, 2755–2781,
565   https://doi.org/10.1175/JCLI-D-11-00316.1, 2012.
566 Demory, M. E., Berthou, S., Fernández, J., Sørland, S. L., Brogli, R., Roberts, M. J.,
567   Beyerle, U., Seddon, J., Haarsma, R., Schär, C., Buonomo, E., Christensen, O. B.,
568   Ciarlo, J. M., Fealy, R., Nikulin, G., Peano, D., Putrasahan, D., Roberts, C. D., Senan,
569   R., Steger, C., Teichmann, C., and Vautard, R.: European daily precipitation according
570   to EURO-CORDEX regional climate models (RCMs) and high-resolution global climate
571   models (GCMs) from the High-Resolution Model Intercomparison Project
572   (HighResMIP), Geosci Model Dev, 13, 5485–5506, https://doi.org/10.5194/gmd-13-
573   5485-2020, 2020.
574 ECMWF: IFS Documentation CY43R3 - Part IV: Physical processes,
575   https://doi.org/10.21957/efyk72kl, 2017.
576 Gori, A., Lin, N., Xi, D., and Emanuel, K.: Tropical cyclone climatology change greatly
577   exacerbates US extreme rainfall–surge hazard, Nat Clim Chang, 12, 171–178,
578   https://doi.org/10.1038/s41558-021-01272-7, 2022.
579 Graham, R. M., Hudson, S. R., and Maturilli, M.: Improved Performance of ERA5 in
580   Arctic Gateway Relative to Four Global Atmospheric Reanalyses, Geophys Res Lett, 46,
581   6138–6147, https://doi.org/10.1029/2019GL082781, 2019.

Hack, J. J., Caron, J. M., Danabasoglu, G., Oleson, K. W., Bitz, C., and Truesdale, J. E.: CCSM-CAM3 Climate Simulation Sensitivity to Changes in Horizontal Resolution, 2006.

Hassler, B. and Lauer, A.: Comparison of reanalysis and observational precipitation datasets including era5 and wfde5, Atmosphere (Basel), 12, https://doi.org/10.3390/atmos12111462, 2021.

Hersbach, H., Bell, B., Berrisford, P., Hirahara, S., Horányi, A., Muñoz-Sabater, J., Nicolas, J., Peubey, C., Radu, R., Schepers, D., Simmons, A., Soci, C., Abdalla, S., Abellan, X., Balsamo, G., Bechtold, P., Biavati, G., Bidlot, J., Bonavita, M., De Chiara, G., Dahlgren, P., Dee, D., Diamantakis, M., Dragani, R., Flemming, J., Forbes, R., Fuentes, M., Geer, A., Haimberger, L., Healy, S., Hogan, R. J., Hólm, E., Janisková, M., Keeley, S., Laloyaux, P., Lopez, P., Lupu, C., Radnoti, G., de Rosnay, P., Rozum, I., Vamborg, F., Villaume, S., and Thépaut, J. N.: The ERA5 global reanalysis, Quarterly Journal of the Royal Meteorological Society, 146, 1999–2049, https://doi.org/10.1002/qj.3803, 2020.

Hersbach, H., Bell, B., Berrisford, P., Biavati, G., Horányi, A., Muñoz Sabater, J., Nicolas, J., Peubey, C., Radu, R., Rozum, I., Schepers, D., Simmons, A., Soci, C., Dee, D., Thépaut, J-N.: ERA5 hourly data on single levels from 1940 to present. Copernicus Climate Change Service (C3S) Climate Data Store (CDS), DOI: 10.24381/cds.adbb2d47, 2023 (Accessed on 16-09-2022).

Hertwig, E., von Storch, J. S., Handorf, D., Dethloff, K., Fast, I., and Krismer, T.: Effect of horizontal resolution on ECHAM6-AMIP performance, Clim Dyn, 45, 185–211, https://doi.org/10.1007/s00382-014-2396-x, 2015.

Hyndman, R. J. and Fan, Y.: Sample Quantiles in Statistical Packages, Source: The American Statistician, 361–365 pp., 1996.

Iles, C. E., Vautard, R., Strachan, J., Joussaume, S., Eggen, B. R., and Hewitt, C. D.: The benefits of increasing resolution in global and regional climate simulations for European climate extremes, Geosci Model Dev, 13, 5583–5607, https://doi.org/10.5194/gmd-13-5583-2020, 2020.

Intergovernmental Panel on Climate Change: Weather and Climate Extreme Events in a Changing Climate, in: Climate Change 2021 – The Physical Science Basis, Cambridge University Press, 1513–1766, https://doi.org/10.1017/9781009157896.013, 2023.

Jones, P. W.: First-and Second-Order Conservative Remapping Schemes for Grids in Spherical Coordinates, 1998.

Jong, B. T., Delworth, T. L., Cooke, W. F., Tseng, K. C., and Murakami, H.: Increases in extreme precipitation over the Northeast United States using high-resolution climate model simulations, NPJ Clim Atmos Sci, 6, https://doi.org/10.1038/s41612-023-00347-w, 2023.

Jung, T., Miller, M. J., Palmer, T. N., Towers, P., Wedi, N., Achuthavarier, D., Adams, J. M., Altshuler, E. L., Cash, B. A., Kinter, J. L., Marx, L., Stan, C., and Hodges, K. I.: High-resolution global climate simulations with the ECMWF model in project athena: Experimental design, model climate, and seasonal forecast skill, J Clim, 25, 3155–3172, https://doi.org/10.1175/JCLI-D-11-00265.1, 2012.

Khairoutdinov, M. and Kogan, Y.: A New Cloud Physics Parameterization in a Large-Eddy Simulation Model of Marine Stratocumulus, 2000.

Kopparla, P., Fischer, E. M., Hannay, C., and Knutti, R.: Improved simulation of extreme precipitation in a high-resolution atmosphere model, Geophys Res Lett, 40, 5803–5808, https://doi.org/10.1002/2013GL057866, 2013.

Kritsikis, E., Aechtner, M., Meurdesoif, Y., and Dubos, T.: Conservative interpolation between general spherical meshes, Geosci Model Dev, 10, 425–431, https://doi.org/10.5194/gmd-10-425-2017, 2017.

Lavers, D. A., Simmons, A., Vamborg, F., and Rodwell, M. J.: An evaluation of ERA5 precipitation for climate monitoring, Quarterly Journal of the Royal Meteorological Society, 148, 3152–3165, https://doi.org/10.1002/qj.4351, 2022.

Li, C., Zwiers, F., Zhang, X., Li, G., Sun, Y., and Wehner, M.: Changes in Annual Extremes of Daily Temperature and Precipitation in CMIP6 Models, J Clim, 34, 3441–3460, https://doi.org/10.1175/JCLI-D-19, 2021.

Li, F., Collins, W. D., Wehner, M. F., Williamson, D. L., Olson, J. G., and Algieri, C.: Impact of horizontal resolution on simulation of precipitation extremes in an aqua-planet version of Community Atmospheric Model (CAM3), n.d.

Malardel, S., Wedi, N., Deconinck, W., and Kühnlein, C.: A new grid for the IFS, 2016.

Manganello, J. V., Hodges, K. I., Kinter, J. L., Cash, B. A., Marx, L., Jung, T., Achuthavarier, D., Adams, J. M., Altshuler, E. L., Huang, B., Jin, E. K., Stan, C., Towers, P., and Wedi, N.: Tropical cyclone climatology in a 10-km global atmospheric GCM: Toward weather-resolving climate modeling, J Clim, 25, 3867–3893, https://doi.org/10.1175/JCLI-D-11-00346.1, 2012.

Masunaga, H., Schröder, M., Furuzawa, F. A., Kummerow, C., Rustemeier, E., and Schneider, U.: Inter-product biases in global precipitation extremes, Environmental Research Letters, 14, https://doi.org/10.1088/1748-9326/ab5da9, 2019.

Mishra, S. K. and Sahany, S.: Effects of time step size on the simulation of tropical climate in NCAR-CAM3, Clim Dyn, 37, 689–704, https://doi.org/10.1007/s00382-011-0994-4, 2011.

Monerie, P. A., Chevuturi, A., Cook, P., Klingaman, N. P., and Holloway, C. E.: Role of atmospheric horizontal resolution in simulating tropical and subtropical South American precipitation in HadGEM3-GC31, Geosci Model Dev, 13, 4749–4771, https://doi.org/10.5194/gmd-13-4749-2020, 2020.

Myhre, G., Alterskjær, K., Stjern, C. W., Hodnebrog, Marelle, L., Samset, B. H., Sillmann, J., Schaller, N., Fischer, E., Schulz, M., and Stohl, A.: Frequency of extreme precipitation increases extensively with event rareness under global warming, Sci Rep, 9, https://doi.org/10.1038/s41598-019-52277-4, 2019.

O'Gorman, P. A.: Precipitation Extremes Under Climate Change, https://doi.org/10.1007/s40641-015-0009-3, 1 June 2015.

Prein, A. F., Gobiet, A., Suklitsch, M., Truhetz, H., Awan, N. K., Keuler, K., and Georgievski, G.: Added value of convection permitting seasonal simulations, Clim Dyn, 41, 2655–2677, https://doi.org/10.1007/s00382-013-1744-6, 2013.

Roberts, C. D., Senan, R., Molteni, F., Boussetta, S., Mayer, M., and Keeley, S. P. E.: Climate model configurations of the ecmwf integrated forecasting system (ecmwf-ifs cycle 43r1) for highresmip, Geosci Model Dev, 11, 3681–3712, https://doi.org/10.5194/gmd-11-3681-2018, 2018.

Savita, A., Kjellsson, J., Kedzierski, R. P., Latif, M., Rahm, T., Wahl, S., and Park, W.: Assessment of climate biases in OpenIFS version 43r3 across model horizontal resolutions and time steps, Geosci Model Dev, 17, 1813–1829, https://doi.org/10.5194/gmd-17-1813-2024, 2024.

Schiemann, R., Demory, M. E., Mizielinski, M. S., Roberts, M. J., Shaffrey, L. C., Strachan, J., and Vidale, P. L.: The sensitivity of the tropical circulation and Maritime Continent precipitation to climate model resolution, Clim Dyn, 42, 2455–2468, https://doi.org/10.1007/s00382-013-1997-0, 2014.

Sillmann, J., Kharin, V. V., Zhang, X., Zwiers, F. W., and Bronaugh, D.: Climate extremes indices in the CMIP5 multimodel ensemble: Part 1. Model evaluation in the present climate, Journal of Geophysical Research Atmospheres, 118, 1716–1733, https://doi.org/10.1002/jgrd.50203, 2013.

Strandberg, G. and Lind, P.: The importance of horizontal model resolution on simulated precipitation in Europe – from global to regional models, Weather and Climate Dynamics, 2, 181–204, https://doi.org/10.5194/wcd-2-181-2021, 2021.

Sundqvist, H.: A parameterization scheme for non-convective condensation including prediction of cloud water content, Quarterly Journal of the Royal Meteorological Society, 104, 677–690, https://doi.org/10.1002/qj.49710444110, 1978.

Tarek, M., Brissette, F. P., and Arsenault, R.: Evaluation of the ERA5 reanalysis as a potential reference dataset for hydrological modelling over North America, Hydrol Earth Syst Sci, 24, 2527–2544, https://doi.org/10.5194/hess-24-2527-2020, 2020.

Tetzner, D., Thomas, E., and Allen, C.: A validation of ERA5 reanalysis data in the southern antarctic peninsula—Ellsworth land region, and its implications for ice core studies, Geosciences (Switzerland), 9, https://doi.org/10.3390/geosciences9070289, 2019.

Torma, C., Giorgi, F., and Coppola, E.: Added value of regional climate modeling over areas characterized by complex terrain-precipitation over the Alps, J Geophys Res, 120, 3957–3972, https://doi.org/10.1002/2014JD022781, 2015.

Wang, C., Graham, R. M., Wang, K., Gerland, S., and Granskog, M. A.: Comparison of ERA5 and ERA-Interim near-surface air temperature, snowfall and precipitation over Arctic sea ice: effects on sea ice thermodynamics and evolution, Cryosphere, 13, 1661–1679, https://doi.org/10.5194/tc-13-1661-2019, 2019.

Wehner, M. F., Smith, R. L., Bala, G., and Duffy, P.: The effect of horizontal resolution on simulation of very extreme US precipitation events in a global atmosphere model, Clim Dyn, 34, 241–247, https://doi.org/10.1007/s00382-009-0656-y, 2010.

Wehner, M. F., Reed, K. A., Li, F., Prabhat, Bacmeister, J., Chen, C. T., Paciorek, C., Gleckler, P. J., Sperber, K. R., Collins, W. D., Gettelman, A., and Jablonowski, C.: The effect of horizontal resolution on simulation quality in the Community Atmospheric Model, CAM5.1, J Adv Model Earth Syst, 6, 980–997, https://doi.org/10.1002/2013MS000276, 2014.

Xu, X., Frey, S. K., Boluwade, A., Erler, A. R., Khader, O., Lapen, D. R., and Sudicky, E.: Evaluation of variability among different precipitation products in the Northern Great Plains, J Hydrol Reg Stud, 24, https://doi.org/10.1016/j.ejrh.2019.100608, 2019.

Zhu, L. and Quiring, S. M.: Exposure to precipitation from tropical cyclones has increased over the continental United States from 1948 to 2019, Commun Earth Environ, 3, https://doi.org/10.1038/s43247-022-00639-8, 2022.

Ziese, Markus; Rauthe-Schöch, Armin; Becker, Andreas; Finger, Peter; Rustemeier, Elke; Hänsel, Stephanie; Schneider, Udo: GPCC Full Data Daily Version 2022 at 1.0°: Daily Land-Surface Precipitation from Rain-Gauges built on GTS-based and Historic Data. DOI: 10.5676/DWD_GPCC/FD_D_V2022_100, 2022

726
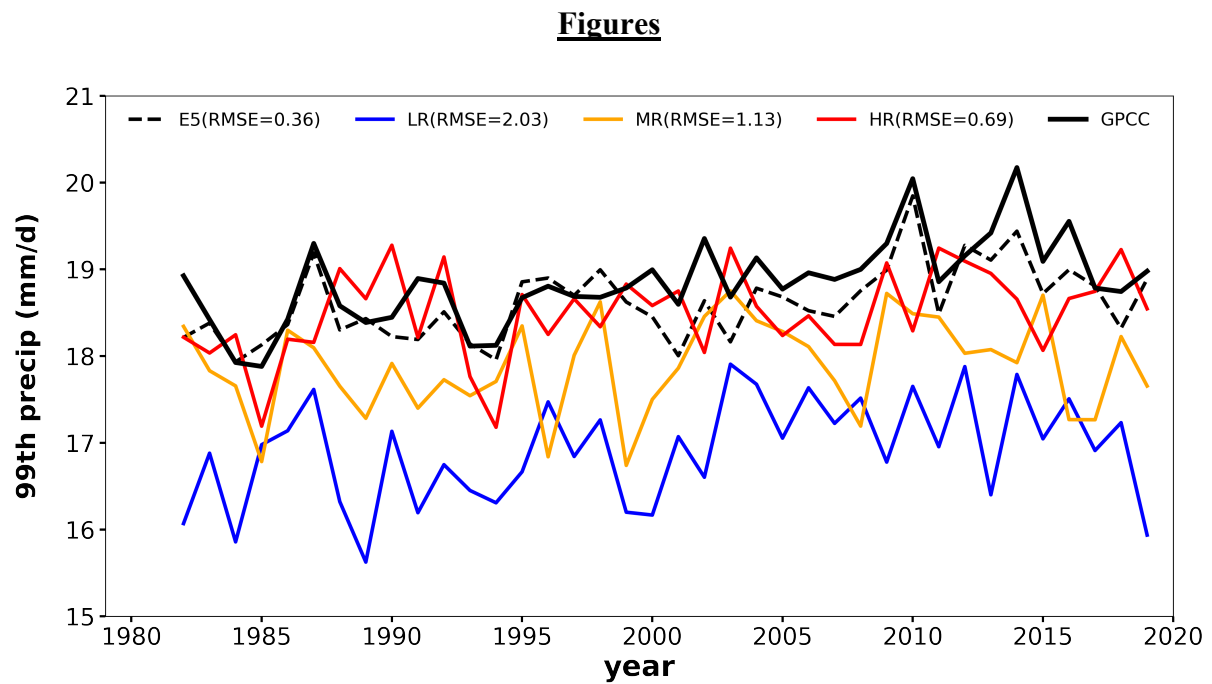
728
729
730   Fig. 1 Annual time series of the 99th percentile precipitation using observations (GPCC, black

731   solid line), reanalysis (ERA5, black dash line), and model simulations (LR: blue, MR: orange,

732   HR: red) during 1982-2019 over Europe. RMSE values of 99th percentile precipitation are

733   computed referenced to GPCC which are shown within the small bracket (unit: mm/d).

734
735
736
737
738
739
740
741
742
743
744
745
746
747
748
749
750
751
752
753
754
755
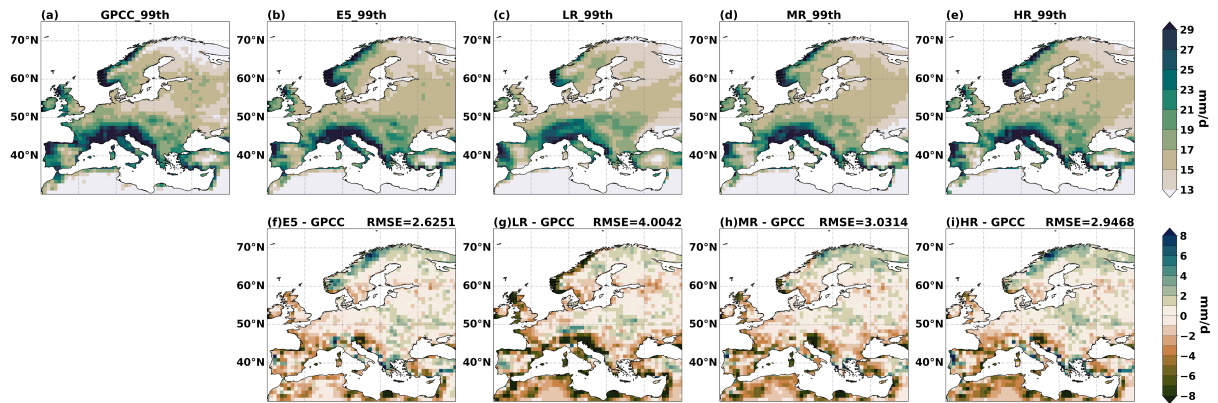
Fig. 2 The 99th percentile precipitation over Europe during 1982-2019 from (a) GPCC observations, (b) ERA5 reanalysis, (c) LR, (d) MR, (e) HR, and the corresponding biases and RMSEs in (f) ERA5, (g) LR, (h) MR, and (i) HR.
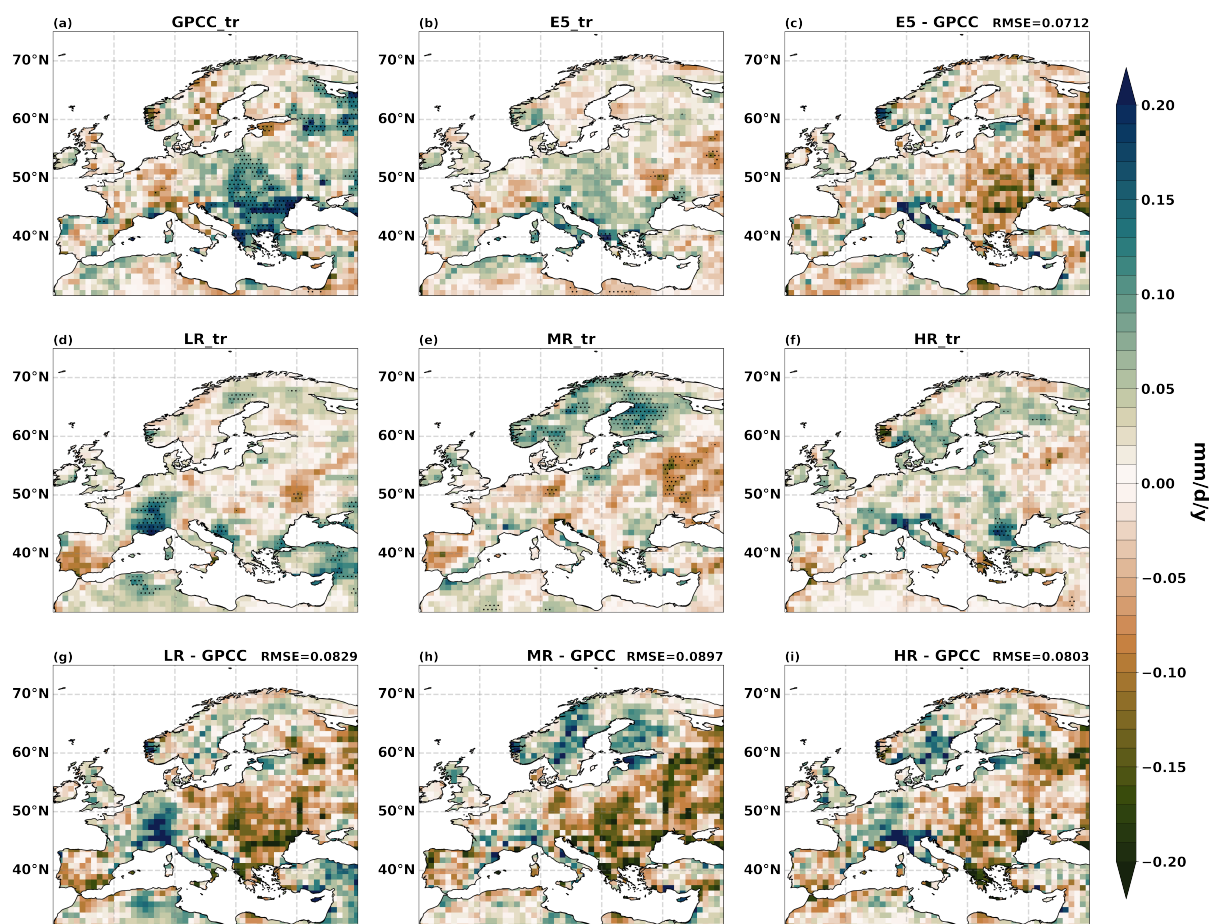
Fig. 3 The linear trends of annual 99th percentile precipitation over Europe during 1982-2019 from (a) GPCC observations, (b) ERA5 reanalysis, (d) LR, (e) MR, (f) HR, and the corresponding biases and RMSEs in (c) ERA5, (g) LR, (h) MR, (i) HR. The shadings are trends at 95 % significance levels.
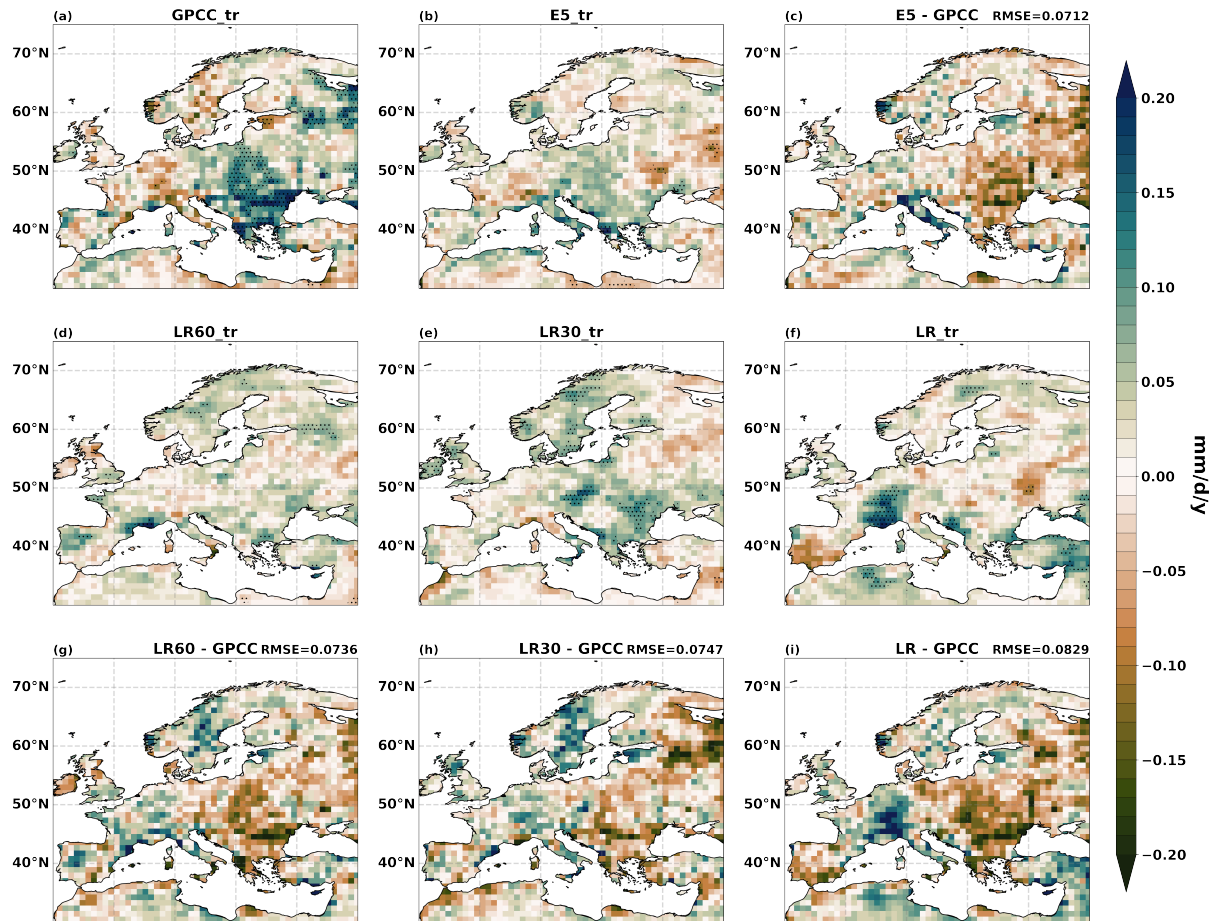
Fig. 4 The linear trends of annual 99th percentile precipitation over Europe during 1982-2019 from (a) GPCC observations, (b) ERA5 reanalysis, (d) LR60m, (e) LR30m, (f) LR, and the corresponding biases and RMSEs in (c) ERA5, (g) LR60m, (h) LR30m, (i) LR. The shadings are trends at 95 % significance levels.

813
814
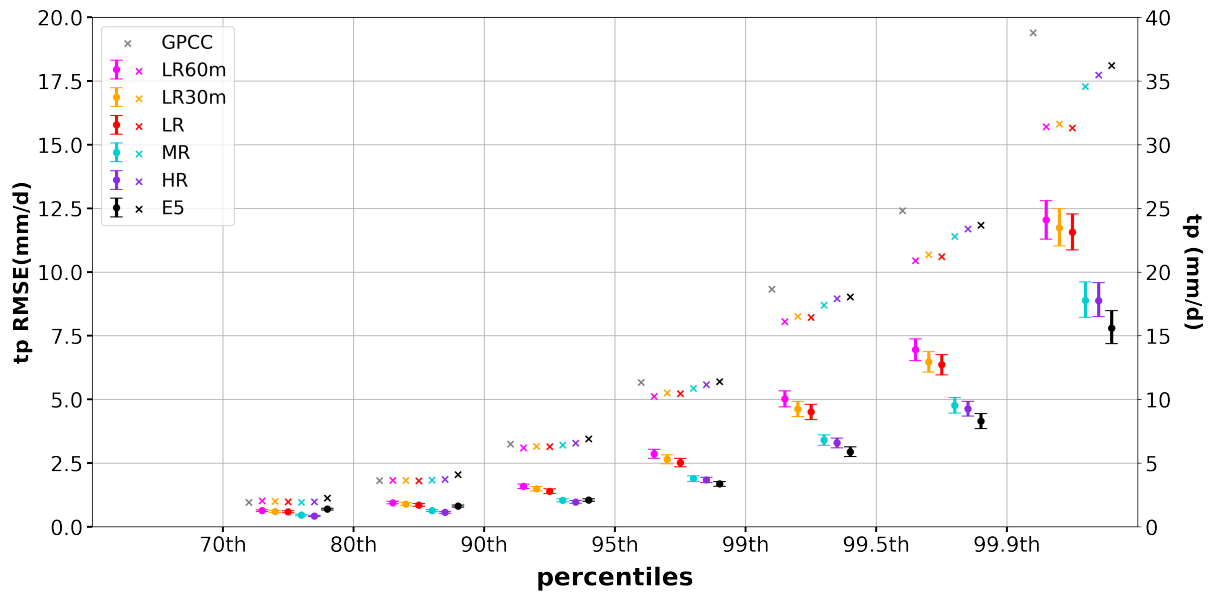
815 Fig. 5 European averaged precipitation amounts and RMSEs (referenced to GPCC) for

816 European total precipitation at different percentile ranges ($70^{th} – 80^{th}$, $80^{th} – 90^{th}$, $90^{th} – 95^{th}$,

817 $95^{th} – 99^{th}$, $99^{th} – 99.5^{th}$, $99.5^{th} – 99.9^{th}$ and $>99.9^{th}$ percentile) in ERA5 (black) and OpenIFS

818 simulations (LR60m: magenta, LR30m: orange, LR: red, MR: blue, HR: purple) during 1982-

819 2019. Cross marks are the precipitation amounts. Dots are the RMSE values, and error bars are

820 the 95 % CI.

821

822

823
824
825
826
827
828
829
830

831
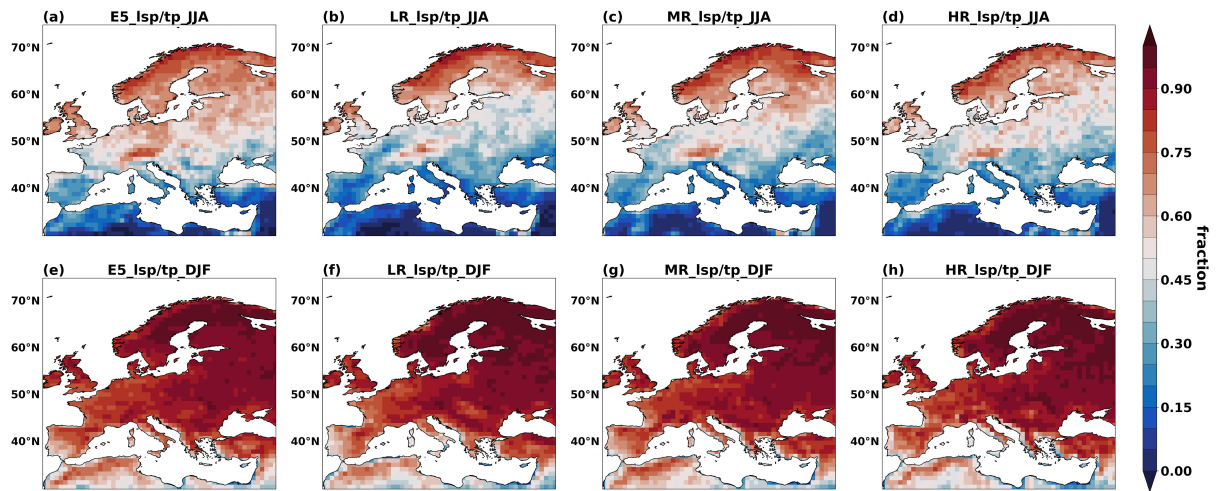
832 Fig. 6 Contribution of large-scale precipitation to extreme precipitation (>99th percentile) in

833 ERA5 (a & e), LR (b & f), MR (c & g) and HR (d & h) over Europe in JJA (a-d) and DJF (e-

834 h) over the period 1982-2019.

835

836

837

838

839

840

841

842

843

844

845

846

847

848
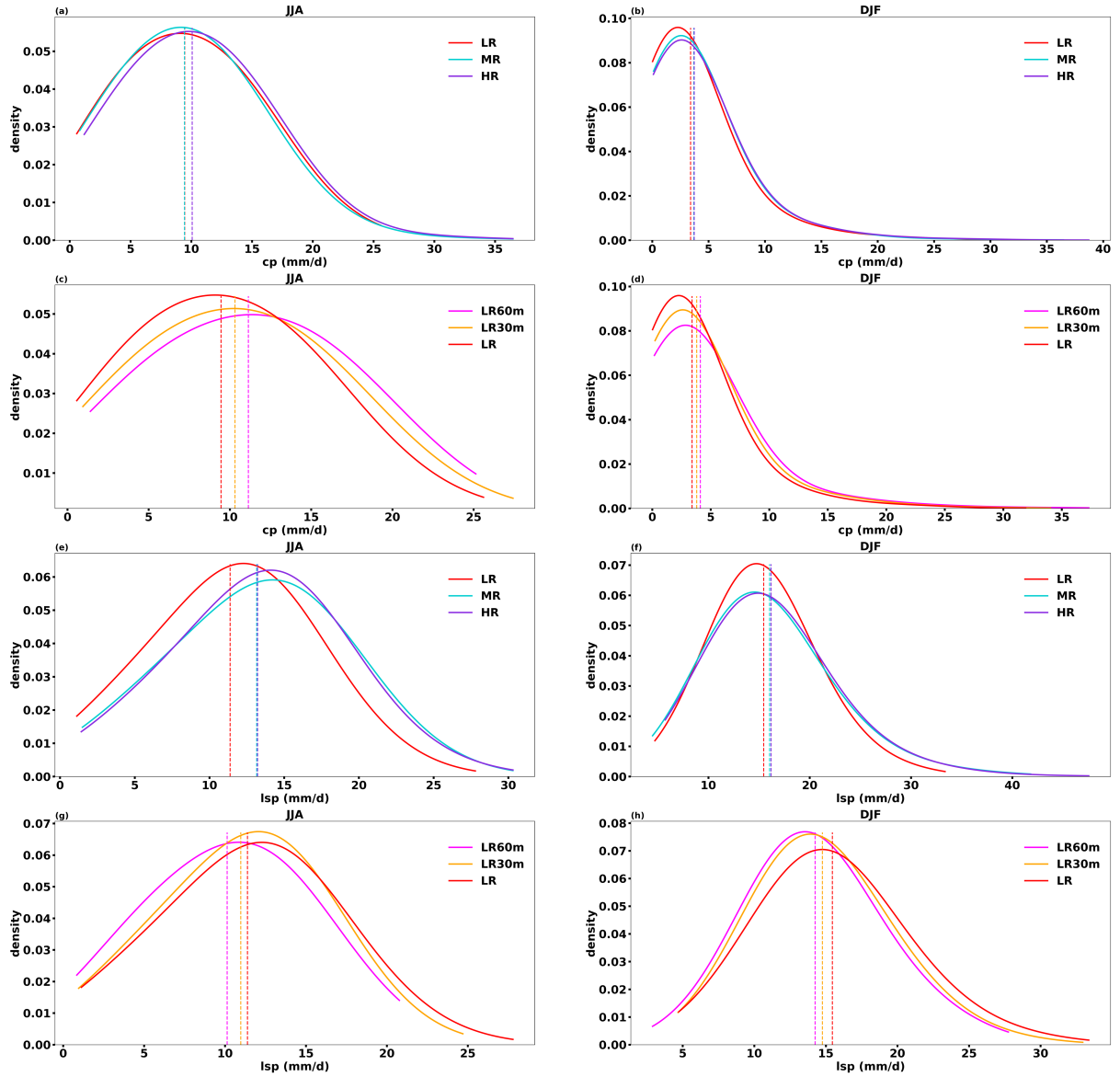
849 Fig. 7 European convective (a-d) and large-scale precipitation (e-h) distribution across different

850 horizontal resolutions (a, b, e and f) and model time steps (c, d, g and h) during extreme

851 precipitation days in JJA and DJF (LR60m: magenta, LR30m: orange, LR: red, MR: blue, HR:

852 purple). The time period is 1982-2019. The dash lines are the mean values of each distribution.

853
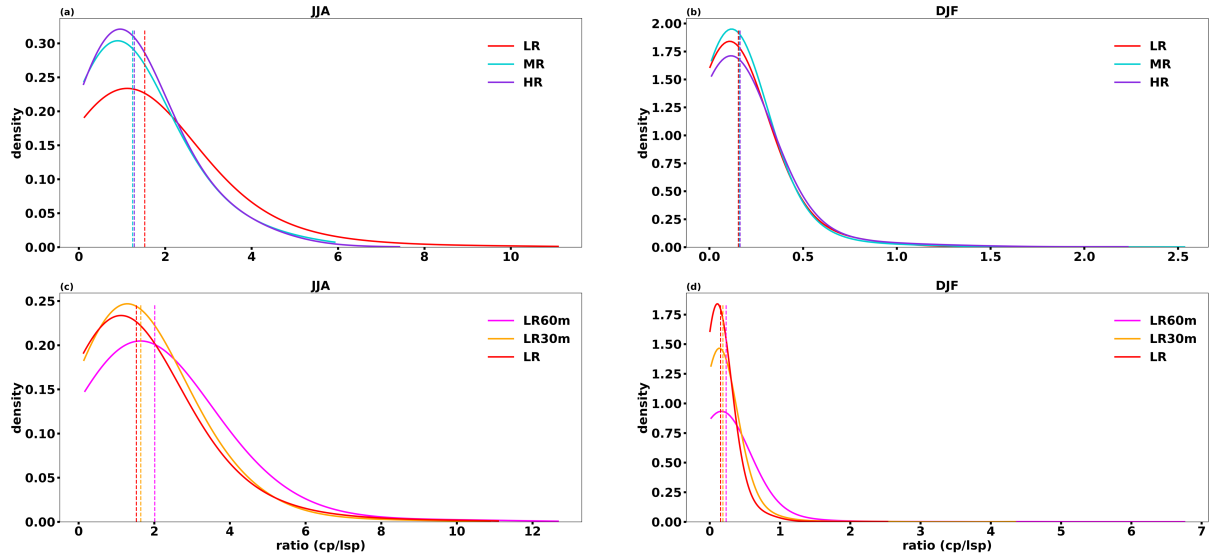
854
855
856 Fig. 8 The ratio between European convective and large-scale precipitation during extreme

857 precipitation days across different horizontal resolutions (a & b) and model time steps (c & d)

858 in JJA and DJF (LR60m: magenta, LR30m: orange, LR: red, MR: blue, HR: purple). The dash

859 lines are the mean values of each distribution.

860
861
862
863
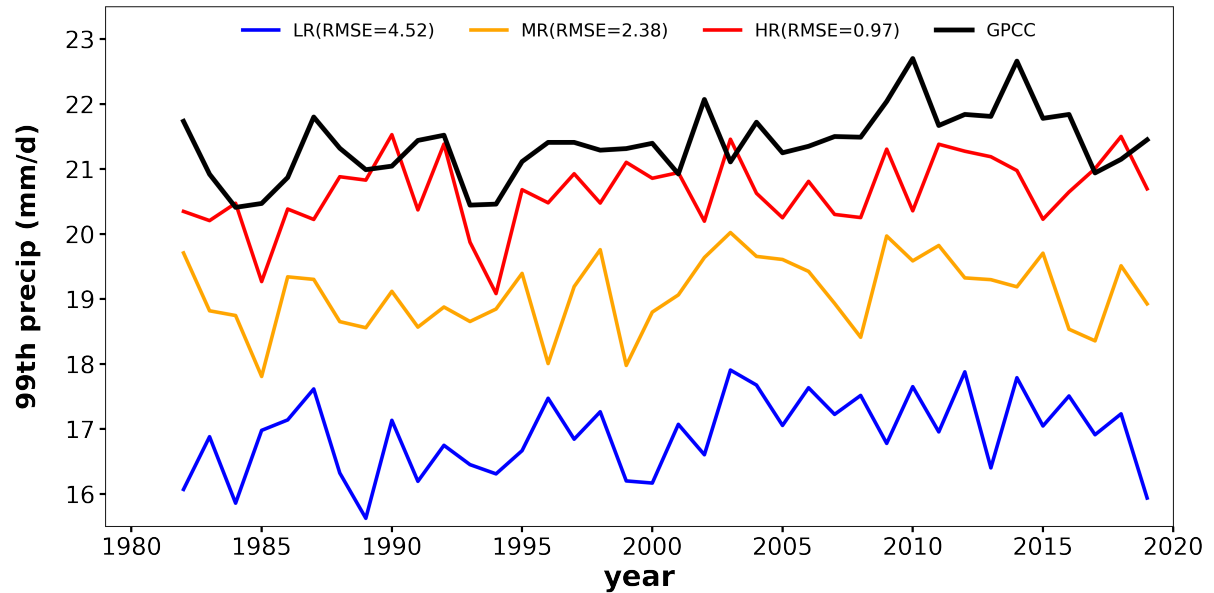
864
865 Fig. 9 Annual time series of the 99th percentile precipitation using observations (GPCC, black

866 solid line) and model simulations on their native resolution (LR: blue, MR: orange, HR: red)

867 during 1982-2019 over Europe. RMSE values of 99th percentile precipitation are computed

868 referenced to GPCC which are shown within the small bracket (unit: mm/d).

869
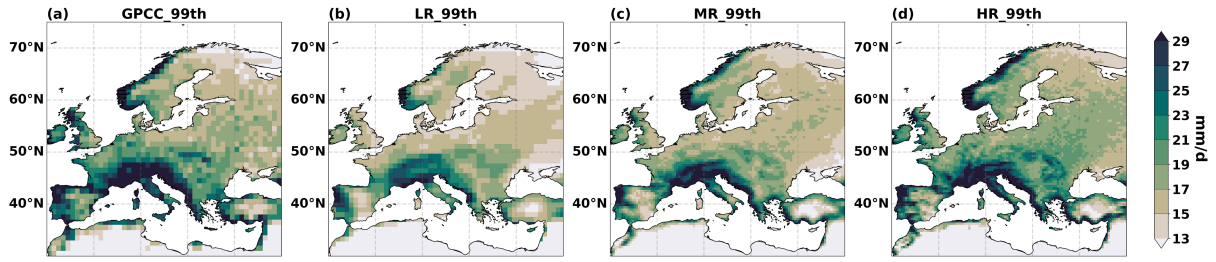
870
871
872 Fig. 10 The 99th percentile precipitation over Europe during 1982-2019 from (a) GPCC

873 observations, (b) LR, (c) MR, (d) HR on their native resolution.

874
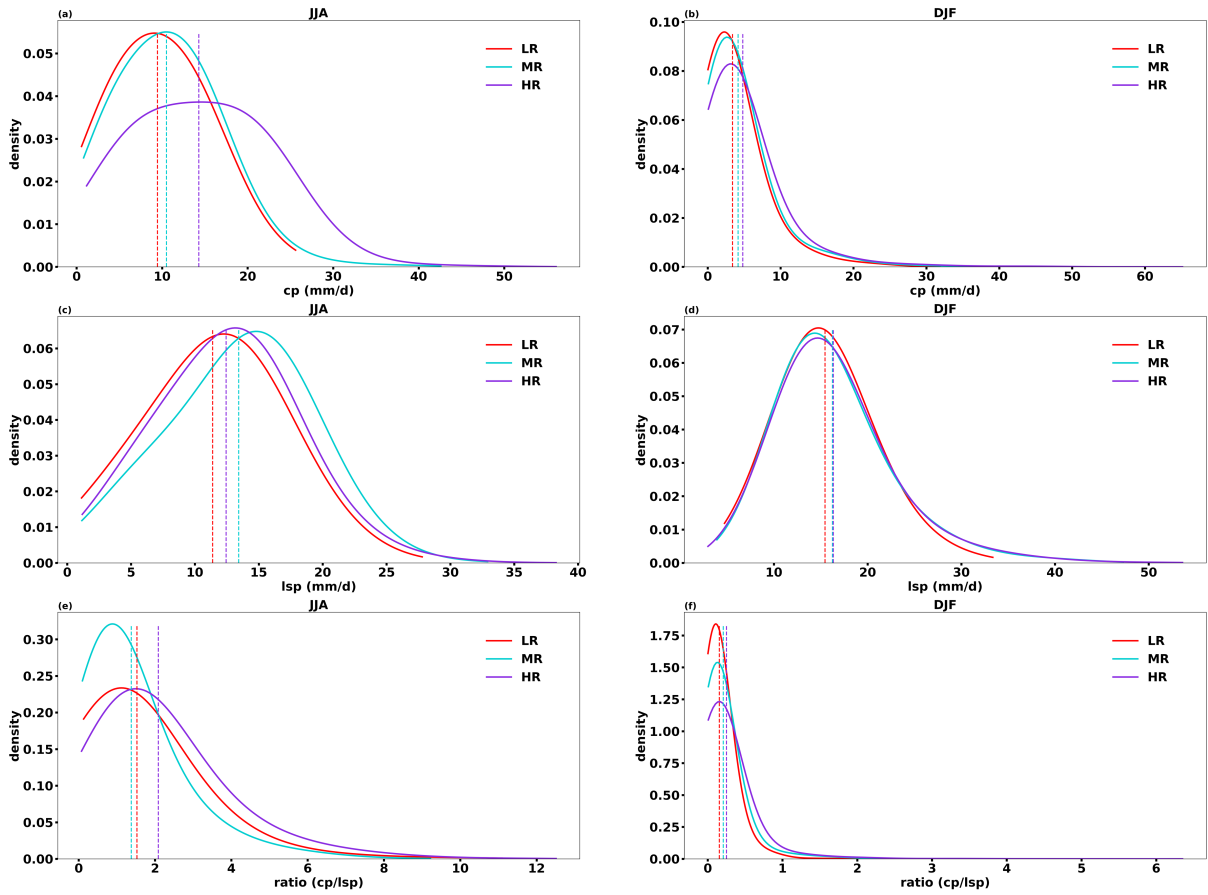
875
876
877 Fig. 11 European convective (a & b), large-scale precipitation (c & d) distribution and ratio

878 (cp/lsp) on their native resolution across different horizontal resolutions during extreme

879 precipitation days in JJA and DJF (LR: red, MR: blue, HR: purple). The time period is 1982-

880 2019. The dash lines are the mean values of each distribution.

881
882
883
884
885
886
887

888
889
890   **Table**

891   Table 1: The experiment details of different horizontal resolutions and model time steps in

892   OpenIFS.

	LR60m	LR30m	LR	MR	HR
Vertical resolution	L91			L91	L91
Horizontal Resolution	100 km (Tco95)			50 km (Tco199)	25 km (Tco399)
Native output resolution	192×384			400×800	800×1600 (400×800 is used in the evaluation)
Regridded resolution	192×384			192×384	192×384
Time steps	60 minutes	30 minutes	15 minutes	15 minutes	15 minutes

893
894
895
896
897
898
899
900
901
902
903
904
905
906
907
908
909

Table 2: The p-values of t-test for convective (Table 2a), large-scale precipitation (Table 2b) and their ratios (Table 2c) distribution across horizontal resolutions and model time steps. The bold means significant (p-value < 0.05).

Table 2a

cp	JJA	DJF
LR → MR	0.92	**0.02**
MR → HR	**2.1 e-4**	0.75
LR60m → LR30m	**4.3 e-6**	**0.02**
LR30m → LR	**5.1 e-7**	**0.001**

Table 2b

lsp	JJA	DJF
LR → MR	**1.8 e-29**	**2.2 e-4**
MR → HR	0.70	0.39
LR60m → LR30m	**3.3 e-9**	**9.4 e-5**
LR30m → LR	**0.005**	**3.0 e-7**

Table 2c

ratio	JJA	DJF
LR → MR	**3.0 e-8**	0.49
MR → HR	0.37	0.64
LR60m → LR30m	**1.6 e-10**	**9.0 e-4**
LR30m → LR	**0.03**	**2.0 e-4**